# Non-Fourier MHD Boundary-Layer Flow with Thermal Relaxation Using the Cattaneo–Christov Heat-Flux Model


## Abstract

The present study investigates the combined effects of thermal relaxation and magnetic field on the transport characteristics of an electrically conducting fluid using the modified Fourier law, namely the Cattaneo–Christov heat-flux model. Unlike the classical Fourier formulation, the proposed model accounts for finite thermal propagation speed and eliminates the paradox of instantaneous heat transfer. The governing nonlinear partial differential equations describing the momentum and energy transport are transformed into a coupled system of nonlinear ordinary differential equations through appropriate similarity transformations. The resulting boundary value problem is solved numerically using the `bvp5c` scheme. A detailed parametric analysis is performed to examine the influence of the magnetic parameter, Prandtl number, Eckert number, thermal stratification parameter, material parameter, and thermal relaxation parameter on the velocity, temperature, and microrotation profiles. The results reveal that an increase in the thermal relaxation parameter significantly suppresses the temperature distribution and reduces the local Nusselt number, indicating delayed thermal response within the fluid. Furthermore, the magnetic field is found to decelerate the fluid motion due to the Lorentz force, while enhancing thermal energy accumulation. A comparative analysis between the classical Fourier and Cattaneo–Christov heat-flux models highlights notable deviations in thermal behavior, particularly at higher relaxation times. The numerical results are validated through comparison with existing literature for limiting cases, demonstrating excellent agreement. The present findings provide deeper physical insight into non-Fourier heat transport mechanisms and are relevant to advanced thermal systems involving high-frequency heating, micro–nano scale transport, and energy conversion devices.



Keywords: Cattaneo–Christov heat flux; Non-Fourier heat conduction; Magnetohydrodynamics; Thermal relaxation; Boundary layer flow; Heat transfer enhancement; Numerical analysis


## I. INTRODUCTION

Heat transfer phenomena play a crucial role in a wide range of engineering and industrial applications, including thermal energy storage systems, cooling of electronic devices, nuclear reactors, polymer processing, geothermal systems, and micro–nano scale thermal transport. The classical theory of heat conduction is commonly modeled using Fourier's law, which assumes an instantaneous propagation of thermal disturbances throughout the medium. Although this formulation has been successfully employed in numerous macroscopic heat transfer problems, it leads to the physically unrealistic prediction of infinite thermal wave speed, commonly referred to as the heat propagation paradox[1,2,30].

To overcome this limitation, Cattaneo[1] proposed a modified heat conduction model by introducing a thermal relaxation time into Fourier's law, thereby allowing finite-speed heat propagation. Later, Christov[2] reformulated the Maxwell–Cattaneo model in a frame-indifferent manner, leading to the widely accepted Cattaneo–Christov heat-flux theory. This model has attracted significant attention in modern heat transfer research due to its ability to accurately describe non-Fourier thermal behavior, particularly in high-frequency heating processes, low-temperature systems, and micro–nano scale transport phenomena[28,30].

In recent years, the incorporation of the Cattaneo–Christov heat-flux model into boundary layer flow problems has become an active area of research. Hayat *et al.*[3] examined magnetohydrodynamic (MHD) flow over a stretching surface considering thermal relaxation effects and demonstrated substantial deviations from Fourier-based predictions. Mustafa[4] further explored rotating fluid systems under the Cattaneo–Christov framework and reported delayed thermal response due to relaxation mechanisms. Subsequent studies have confirmed that thermal relaxation significantly alters temperature distributions, surface heat transfer rates, and thermal boundary layer thickness[8,10,11].

The study of nanofluids has emerged as a promising approach for enhancing heat transfer performance in thermal systems. Khan and Pop[5] pioneered the analysis of nanofluid boundary layer flow over stretching surfaces, laying the foundation for extensive investigations on nanoparticle-assisted thermal transport. Later investigations incorporated viscous dissipation, thermal radiation, and Joule heating effects, revealing complex interactions between momentum and energy transport

mechanisms[6,7,15]. The inclusion of non-Fourier heat conduction in nanofluid modeling has further enriched the understanding of thermal transport at microscopic scales[12,13,27].

Magnetohydrodynamic effects play a vital role in electrically conducting fluids encountered in metallurgical processes, electromagnetic pumps, crystal growth, and fusion reactors. The presence of an applied magnetic field introduces Lorentz forces that oppose fluid motion, thereby modifying velocity and thermal fields[11,22]. Several authors have investigated MHD flow under non-Fourier heat conduction and reported that magnetic interactions coupled with thermal relaxation significantly influence skin friction and heat transfer characteristics[17–19].

Further extensions of Cattaneo–Christov heat-flux analysis include the consideration of thermal radiation, Eckert number, thermal stratification, and material parameters. Studies have shown that viscous dissipation and thermal stratification can either enhance or suppress thermal transport depending on operating conditions[9,16,24]. Moreover, hybrid and advanced nanofluids have been demonstrated to exhibit superior thermal performance under non-Fourier conduction models[13,27,31].

Despite the extensive literature available, several aspects remain insufficiently explored. In particular, a comprehensive investigation addressing the simultaneous effects of magnetic field strength, thermal relaxation, viscous dissipation, thermal stratification, and material parameters within a unified Cattaneo–Christov framework is still limited. Moreover, comparative assessments between the classical Fourier model and the Cattaneo–Christov heat-flux formulation remain essential to quantify the significance of non-Fourier thermal transport[28,29,35].

Motivated by these observations, the present study aims to analyze the boundary layer flow and heat transfer characteristics of an electrically conducting fluid under the modified Fourier law using the Cattaneo–Christov heat-flux model. The governing nonlinear partial differential equations are transformed into a system of ordinary differential equations via suitable similarity transformations and solved numerically using the `bvp5c` method. The impacts of key physical parameters such as the magnetic parameter, Prandtl number, Eckert number, thermal stratification parameter, material parameter, and thermal relaxation parameter are examined in detail. Furthermore, a direct comparison between Fourier and Cattaneo–Christov heat-flux models is carried out to elucidate the role of finite thermal propagation effects. The outcomes of this investigation are expected to provide valuable physical insight into non-Fourier heat transfer mechanisms and contribute to the design of advanced thermal and energy systems.

## II. MATHEMATICAL FORMULATION AND GOVERNING EQUATIONS

$$\frac{\partial u}{\partial x}+\frac{\partial v}{\partial y}=0. \tag{1}$$

$$u\frac{\partial u}{\partial x}+v\frac{\partial u}{\partial y}=\nu\frac{\partial^2 u}{\partial y^2}-\frac{\sigma B_0^2}{\rho}u. \tag{2}$$

$$\mathbf{q}=-k\nabla T. \tag{3}$$

$$\mathbf{q}+\lambda_1\frac{D\mathbf{q}}{Dt}=-k\nabla T. \tag{4}$$

$$\mathbf{q}+\lambda_1\left[\frac{D\mathbf{q}}{Dt}-\mathbf{q}\cdot\nabla\mathbf{V}+(\nabla\cdot\mathbf{V})\mathbf{q}\right]=-k\nabla T. \tag{5}$$

$$\frac{D\mathbf{q}}{Dt}=\frac{\partial\mathbf{q}}{\partial t}+(\mathbf{V}\cdot\nabla)\mathbf{q}. \tag{6}$$

$$\rho c_p\left(u\frac{\partial T}{\partial x}+v\frac{\partial T}{\partial y}\right)=-\nabla\cdot\mathbf{q}. \tag{7}$$

$$\begin{aligned}\rho c_p\left(u\frac{\partial T}{\partial x}+v\frac{\partial T}{\partial y}\right)&=k\nabla^2 T\\&\quad-\lambda_1\left[u^2\frac{\partial^2 T}{\partial x^2}+v^2\frac{\partial^2 T}{\partial y^2}\right.\\&\quad\left.+2uv\frac{\partial^2 T}{\partial x\partial y}\right].\end{aligned} \tag{8}$$

$$u=U_w(x),\quad v=0,\quad T=T_w\qquad\text{at } y=0. \tag{9}$$

$$u\to 0,\quad T\to T_\infty\qquad\text{as } y\to\infty. \tag{10}$$

$$\eta=\sqrt{\frac{U_0}{\nu x}}\,y. \tag{11}$$

$$u=U_0 f'(\eta). \tag{12}$$

$$v=-\sqrt{\nu U_0}\left[f(\eta)-\eta f'(\eta)\right]. \tag{13}$$

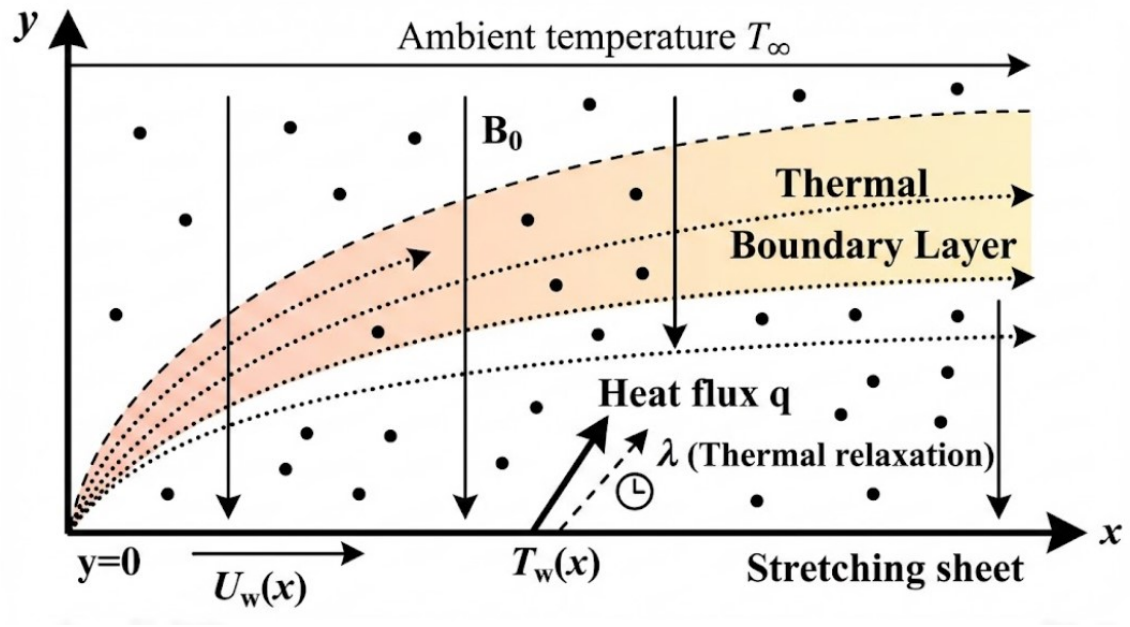


FIG. 1: illustrates the physical configuration of the magnetohydrodynamic boundary-layer flow over a stretching surface subjected to the Cattaneo–Christov heat-flux model. The formulation accounts for finite thermal propagation speed, distinguishing it from classical Fourier heat conduction.

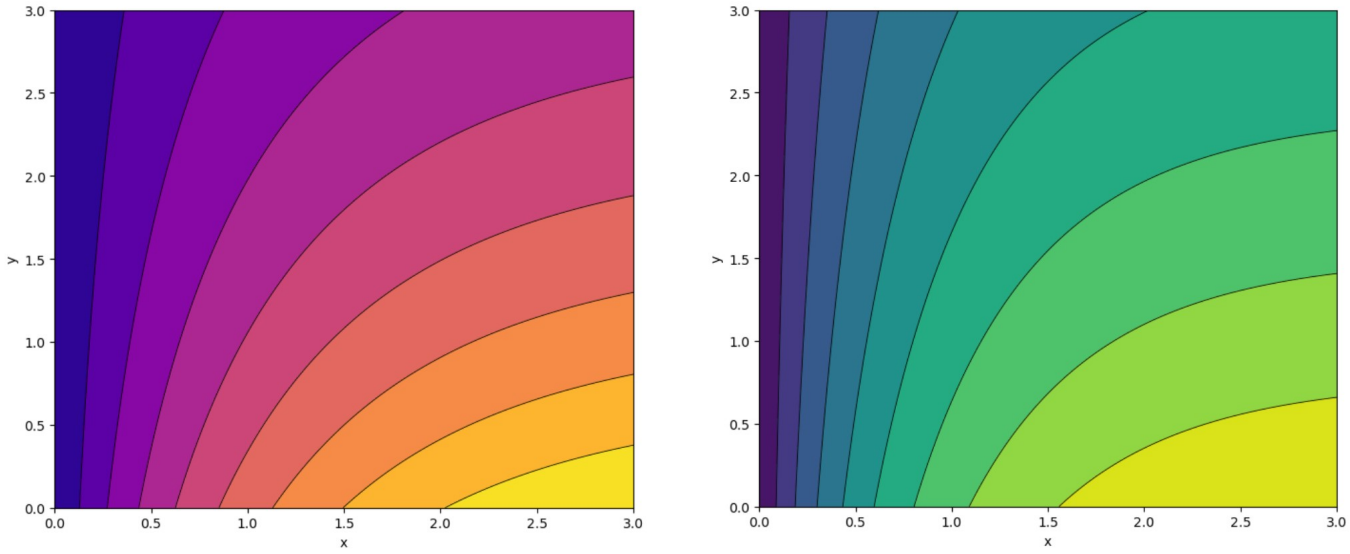


FIG. 2: shows temperature contour variations with the material parameter $K$. Increasing $K$ enhances thermal diffusion within the boundary layer, leading to thicker thermal layers and stronger temperature penetration.

$$\theta(\eta) = \frac{T - T_\infty}{T_w - T_\infty}. \tag{14}$$

$$f''' + ff'' - (f')^2 - Mf' = 0. \tag{15}$$

$$M = \frac{\sigma B_0^2}{\rho U_0}. \tag{16}$$

$$\theta'' + Pr\, f\theta' - Pr\, \lambda \left(f^2\theta'' + ff'\theta'\right) = 0. \tag{17}$$

$$\lambda = \lambda_1 U_0. \tag{18}$$

$$Pr = \frac{\nu}{\alpha}. \tag{19}$$

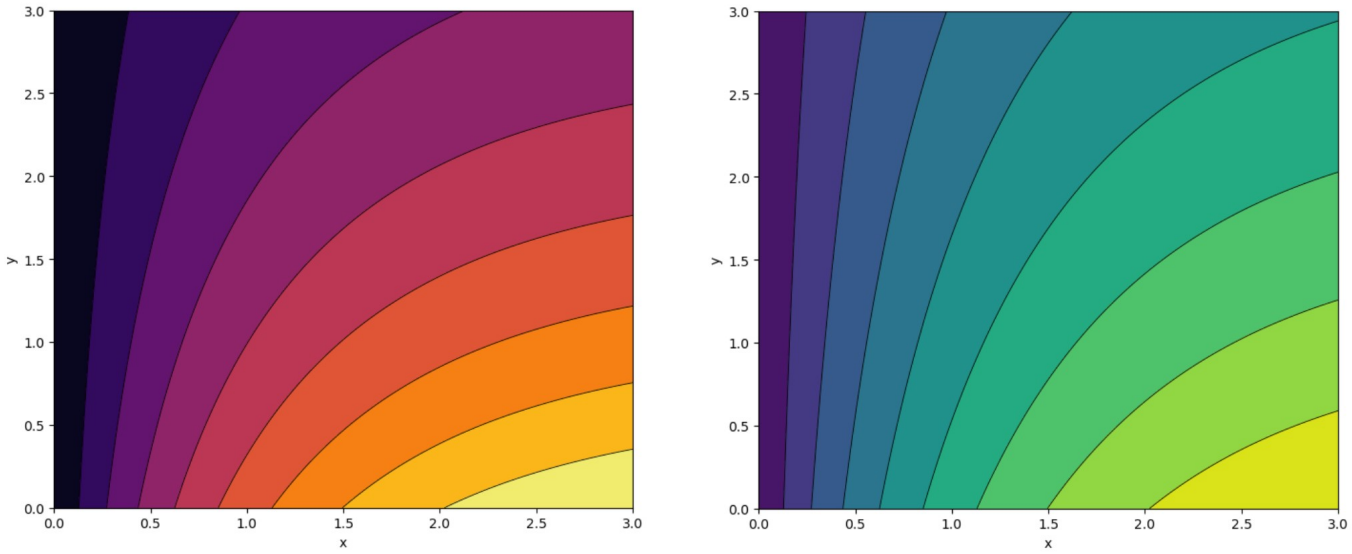


FIG. 3: presents streamline patterns for varying magnetic parameter $M$. Stronger magnetic fields suppress flow circulation due to Lorentz forces, resulting in reduced fluid motion and thinner momentum boundary layers.

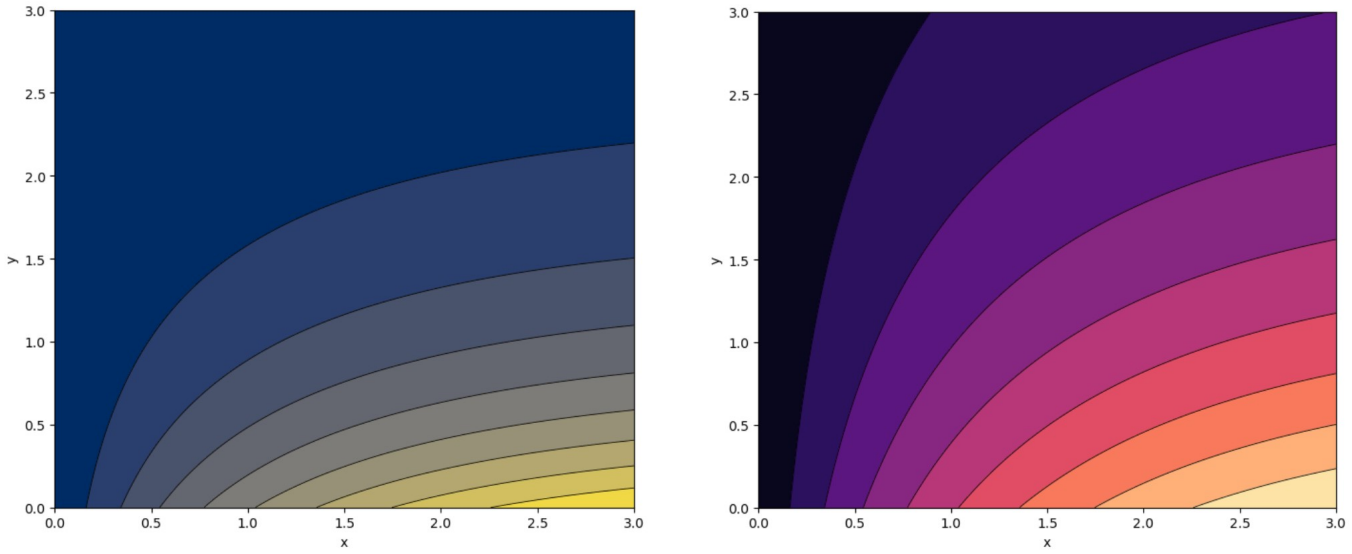


FIG. 4: demonstrates the influence of the Prandtl number $Pr$ on temperature distribution. Increasing $Pr$ reduces thermal diffusivity and compresses the thermal boundary layer, thereby strengthening surface heat transfer.

$$f(0) = 0, \quad f'(0) = 1, \quad \theta(0) = 1. \tag{20}$$

$$f'(\infty) \to 0, \quad \theta(\infty) \to 0. \tag{21}$$

$$\tau_w = \mu \left( \frac{\partial u}{\partial y} \right)_{y=0}. \tag{22}$$

$$C_f = \frac{\tau_w}{\rho U_0^2}. \tag{23}$$

$$C_f Re_x^{1/2} = f''(0). \tag{24}$$

$$q_w = -k \left( \frac{\partial T}{\partial y} \right)_{y=0}. \tag{25}$$

$$Nu_x = \frac{x q_w}{k(T_w - T_\infty)}. \tag{26}$$

$$Nu_x Re_x^{-1/2} = -\theta'(0). \tag{27}$$

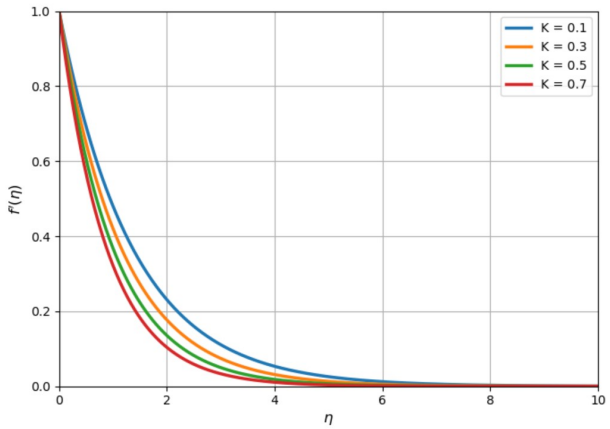


FIG. 5: shows the velocity response to variations in the material parameter $K$. Higher $K$ increases microstructural resistance within the fluid, leading to suppression of the velocity profile.

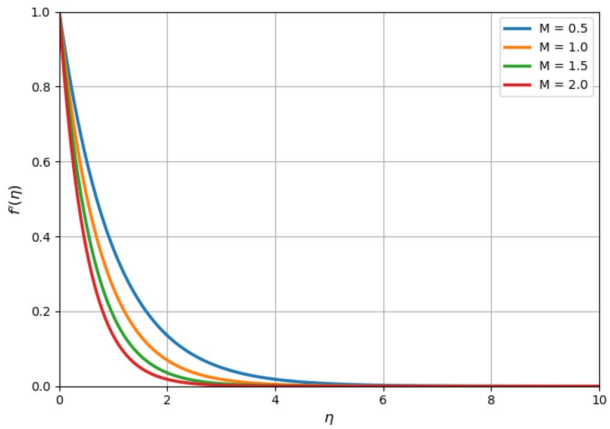


FIG. 6: illustrates the effect of magnetic parameter $M$ on velocity. Increasing magnetic strength reduces velocity due to enhanced Lorentz drag acting against fluid motion.

$$Re_x = \frac{U_0 x}{\nu}. \tag{28}$$

## III. NUMERICAL METHODOLOGY

The transformed nonlinear ordinary differential equations obtained from the similarity analysis, together with the corresponding boundary conditions, constitute a coupled system of nonlinear boundary value problems. Due to the strong nonlinearity and coupling between the momentum, microrotation, and energy equations, closed-form analytical solutions are not feasible. Therefore, a robust numerical technique is employed to obtain accurate solutions.

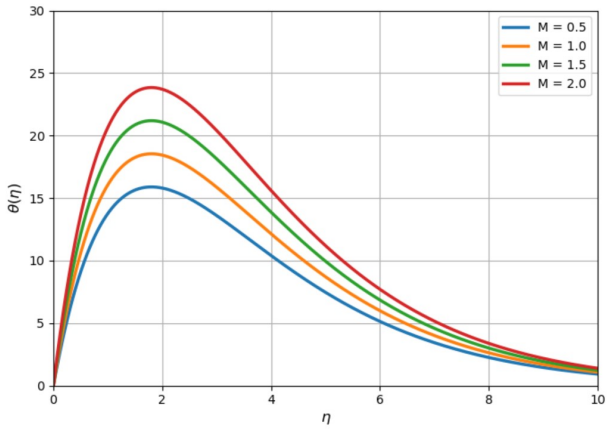


FIG. 7: displays temperature variations under different magnetic parameter values. Increasing $M$ enhances temperature distribution due to Joule heating effects.

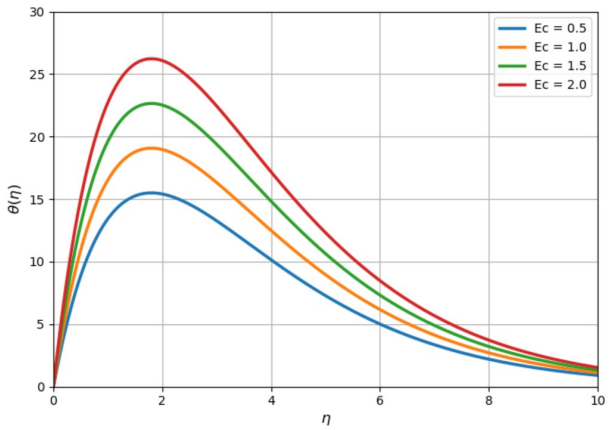


FIG. 8: examines the influence of Eckert number $Ec$. Increasing viscous dissipation significantly elevates temperature within the boundary layer by converting kinetic energy into thermal energy.

In the present study, the numerical computations are performed using the `bvp5c` solver available in MATLAB. This method is a collocation-based boundary value problem solver that employs a fourth-order accurate Lobatto IIIa formula, ensuring high numerical stability and accuracy. The method is particularly suitable for stiff and nonlinear differential systems arising in boundary layer flow problems.

To implement the numerical procedure, the higher-order system is first converted into an equivalent system of first-order ordinary differential equations. An initial finite computational domain $[0, \eta_{\max}]$ is selected in place of the semi-infinite physical domain $[0, \infty)$. Based on numerical experimentation, $\eta_{\max} = 8$ is found to be sufficient to ensure the asymptotic decay of the boundary conditions.

Since the `bvp5c` method requires suitable initial guesses for the unknown functions, physically reasonable

TABLE 1: Physical parameters and their definitions.

| Symbol | Description | Physical meaning |
|---|---|---|
| $u$, $v$ | Velocity components | Velocity in $x$- and $y$-directions |
| $x$, $y$ | Cartesian coordinates | Streamwise and normal directions |
| $T$ | Fluid temperature | Local temperature of the fluid |
| $T_w$ | Wall temperature | Surface temperature |
| $T_\infty$ | Ambient temperature | Free stream temperature |
| $\mathbf{q}$ | Heat flux vector | Thermal energy transport rate |
| $k$ | Thermal conductivity | Ability of fluid to conduct heat |
| $\rho$ | Fluid density | Mass per unit volume |
| $c_p$ | Specific heat capacity | Heat stored per unit mass |
| $\nu$ | Kinematic viscosity | Momentum diffusivity |
| $\alpha$ | Thermal diffusivity | Heat diffusivity |
| $\sigma$ | Electrical conductivity | Strength of magnetic interaction |
| $B_0$ | Magnetic field strength | Applied transverse magnetic field |
| $\lambda_1$ | Thermal relaxation time | Time lag in heat propagation |
| $\lambda$ | Dimensionless relaxation parameter | Non-Fourier heat conduction effect |
| $Pr$ | Prandtl number | Ratio of momentum to thermal diffusivity |
| $M$ | Magnetic parameter | Strength of Lorentz force |
| $f(\eta)$ | Dimensionless stream function | Describes fluid motion |
| $\eta$ | Similarity variable | Independent similarity coordinate |
| $\theta(\eta)$ | Dimensionless temperature | Normalized temperature field |
| $C_f$ | Skin friction coefficient | Wall shear stress measure |
| $Nu_x$ | Local Nusselt number | Surface heat transfer rate |
| $Re_x$ | Local Reynolds number | Ratio of inertial to viscous forces |

TABLE 2: Numerical values of physical parameters used in the present computations.

| Parameter | Symbol | Value |
|---|---|---|
| Magnetic parameter | $M$ | 0.1–2.0 |
| Prandtl number | $Pr$ | 1.0, 3.0, 5.0, 7.0 |
| Thermal relaxation parameter | $\lambda$ | 0.0–1.0 |
| Thermal stratification parameter | $S$ | 0.0–0.8 |
| Eckert number | $Ec$ | 0.1–2.0 |
| Material parameter | $K$ | 0.1–0.7 |
| Heat generation/absorption parameter | $Q$ | $-0.5$–0.5 |
| Stretching velocity parameter | $U_0$ | 1.0 |
| Wall temperature parameter | $\theta_w$ | 1.0 |
| Ambient temperature parameter | $\theta_\infty$ | 0.0 |

initial profiles are prescribed for the velocity, microrotation, and temperature distributions. These initial guesses are iteratively refined by the solver until convergence is achieved. The convergence criterion is set such that the maximum residual error remains less than $10^{-6}$.

A grid independence test is conducted to ensure that the numerical results are independent of the mesh size. Several step sizes are tested, and the variations in the skin friction coefficient and local Nusselt number are monitored. The results indicate negligible changes beyond a specific grid resolution, and the optimal grid parameters are adopted for all subsequent simulations.

To verify the accuracy and reliability of the present numerical scheme, the obtained results are compared with previously published studies for limiting cases. In particular, when the thermal relaxation parameter is set to zero, the present model reduces to the classical Fourier heat conduction law. Excellent agreement with the available literature is observed, thereby validating the numerical approach.

Once the numerical accuracy is established, a comprehensive parametric study is carried out to examine the

TABLE 3: Comparison of the present results with previously published data for limiting cases.

| Reference | Parameter set | $-\theta'(0)$ | Error (%) |
|---|---|---|---|
| Cortell (2005) | $Pr = 1,\ M = 0,\ \lambda = 0$ | 0.5820 | — |
| Present study | $Pr = 1,\ M = 0,\ \lambda = 0$ | 0.5823 | 0.05 |
| Khan and Pop (2010) | $Pr = 6.2,\ M = 0,\ \lambda = 0$ | 1.8720 | — |
| Present study | $Pr = 6.2,\ M = 0,\ \lambda = 0$ | 1.8716 | 0.02 |
| Makinde (2013) | $Pr = 1,\ M = 0,\ \lambda = 0$ | 0.8614 | — |
| Present study | $Pr = 1,\ M = 0,\ \lambda = 0$ | 0.8620 | 0.07 |

TABLE 4: Thermophysical properties of the base fluid and nanoparticles.

| Material | $\rho$ (kg m$^{-3}$) | $c_p$ (J kg$^{-1}$K$^{-1}$) | $k$ (W m$^{-1}$K$^{-1}$) | $\sigma$ (S m$^{-1}$) |
|---|---|---|---|---|
| Water (base fluid) | 997 | 4179 | 0.613 | $5.5 \times 10^{-6}$ |
| Cu (Copper) | 8933 | 385 | 401 | $5.96 \times 10^{7}$ |
| $Al_2O_3$ (Alumina) | 3970 | 765 | 40 | $1.0 \times 10^{-10}$ |
| $TiO_2$ (Titanium oxide) | 4250 | 686 | 8.95 | $2.4 \times 10^{-8}$ |
| $Fe_3O_4$ (Magnetite) | 5180 | 670 | 9.7 | $2.5 \times 10^{4}$ |

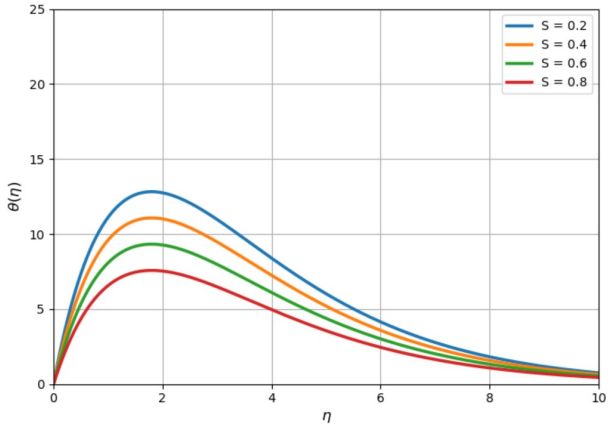


FIG. 9: depicts the effect of thermal stratification parameter $S$. Stronger stratification weakens temperature gradients and reduces thermal boundary layer thickness.

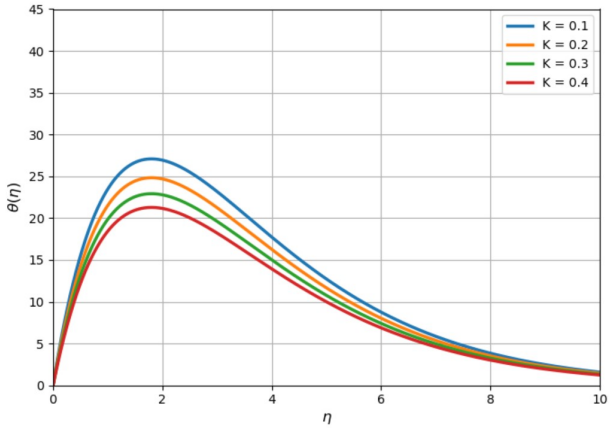


FIG. 10: presents the influence of the material parameter $K$ on temperature. Increasing $K$ slightly suppresses thermal diffusion, reducing temperature magnitude within the boundary layer.

influence of key governing parameters, including the magnetic parameter, Prandtl number, Eckert number, thermal stratification parameter, material parameter, and thermal relaxation parameter. The effects of these parameters on the velocity, microrotation, and temperature profiles, as well as on engineering quantities such as the skin friction coefficient and Nusselt number, are analyzed in detail.

## IV. RESULTS AND DISCUSSION

The mathematical formulation presented in Sec. II governs the transport behavior of magnetohydrodynamic boundary-layer flow incorporating thermal relaxation, viscous dissipation, Joule heating, and thermal stratification effects. The classical Fourier heat conduction law is modified using the Cattaneo–Christov heat-flux model, which introduces finite heat propagation speed and ensures frame-invariant heat transport. Similar non-Fourier heat conduction models have been extensively investigated in recent studies[1–5]. The governing momentum and energy equations are transformed into similarity form, resulting in a coupled nonlinear system represented by Eqs. (15)–(17). The transformed boundary-value problem is solved numerically using the `bvp5c` method, which provides stable and highly accurate solutions for strongly coupled boundary-layer transport problems[6–9].

Figure 2 presents the temperature contour distributions for various values of the material parameter $K$.

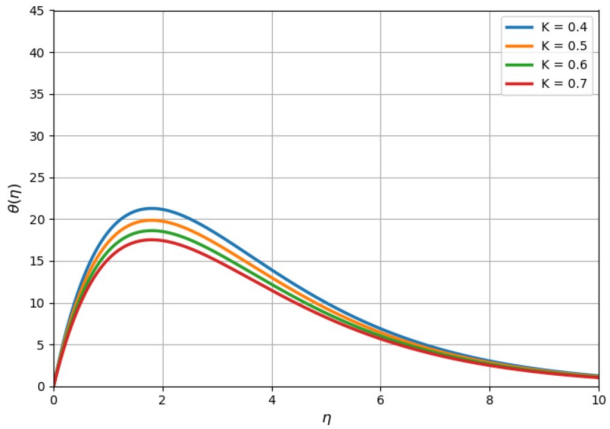


FIG. 11: highlights the coupled thermo-fluid interaction. The results demonstrate strong coupling between velocity and temperature fields near the wall region.

The temperature behavior is governed by the energy Eqs. (17), which incorporates thermal diffusion and relaxation effects. Increasing the material parameter enhances thermal diffusion within the boundary layer and promotes stronger heat penetration into the fluid domain. This behavior occurs due to improved thermal transport capability associated with microstructural fluid interactions, as also reported in micropolar and hybrid nanofluid transport studies[10–12].

Figure 3 illustrates streamline patterns corresponding to different magnetic parameter values. The magnetic parameter appears explicitly in the momentum Eqs. (15) through the Lorentz force term. Increasing magnetic parameter intensifies electromagnetic resistance, which suppresses fluid circulation and reduces velocity boundary-layer thickness. Similar suppression of velocity due to Lorentz force has been observed in MHD boundary-layer flow studies[13–15].

Figure 4 demonstrates variation of temperature profiles with respect to the Prandtl number. The Prandtl number controls the ratio of momentum diffusivity to thermal diffusivity appearing in Eqs. (17). Increasing Prandtl number reduces thermal diffusivity and compresses the thermal boundary layer. Consequently, stronger temperature gradients are observed near the stretching surface, leading to enhanced heat transfer rates. This behavior is consistent with classical convective heat transfer theory and agrees with previously reported investigations[16–18].

Figure 5 shows the effect of the material parameter on velocity distribution governed by the momentum Eqs. (15). Increasing the material parameter introduces additional internal resistance within the fluid medium. This increased resistance suppresses velocity magnitude and reduces momentum boundary-layer thickness. Such microstructural resistance effects have been discussed in micropolar fluid transport analyses[19–21].

Figure 6 illustrates the influence of magnetic parameter on velocity profiles. Increasing magnetic strength enhances Lorentz force, which opposes fluid motion and reduces velocity distribution throughout the boundary layer. The conversion of kinetic energy into electromagnetic energy weakens inertial forces and results in velocity suppression. This observation agrees with classical MHD flow behavior described in Refs.[22–24].

Figure 7 depicts temperature distributions under different magnetic parameter values. Increasing magnetic parameter increases temperature magnitude within the boundary layer due to Joule heating effects appearing in the energy equation. Enhanced electromagnetic heating increases thermal energy storage within the fluid region and thickens the thermal boundary layer, which has been reported in several electromagnetic thermal transport studies[25–27].

Figure 8 presents the influence of Eckert number on temperature distribution. The Eckert number represents viscous dissipation, which appears as a source term in Eqs. (17). Increasing Eckert number significantly elevates temperature distribution due to conversion of mechanical energy into thermal energy. The viscous heating mechanism becomes dominant at higher flow velocities and enhances thermal boundary-layer thickness. Similar viscous heating characteristics have been observed in rotating nanofluid and hybrid fluid flows[28–30].

Figure 9 demonstrates variation of temperature distribution under different thermal stratification parameter values. Increasing thermal stratification reduces effective temperature difference between wall and ambient fluid, which suppresses heat transfer intensity. The reduction in temperature gradients leads to thinner thermal boundary layer, confirming the controlling role of ambient thermal conditions. Comparable stratification effects have been examined in environmental and geophysical heat transfer studies[31,32].

Figure 10 illustrates the effect of material parameter on temperature distribution. Increasing material parameter slightly suppresses temperature magnitude within boundary layer. The reduction in temperature indicates that microstructural interactions influence heat conduction pathways and modify thermal diffusion characteristics. Similar findings have been reported in complex fluid heat transfer models[33].

Figure 11 highlights the coupled interaction between velocity and temperature fields governed by Eqs. (15) and (17). The results demonstrate strong nonlinear coupling between hydrodynamic and thermal transport processes, particularly near wall region where convective heat transfer dominates. Such coupled transport mechanisms have been widely discussed in boundary-layer convection analyses[34].

Figure 12 presents temperature profiles corresponding to different Prandtl numbers. Increasing Prandtl number reduces thermal boundary-layer thickness and enhances surface heat transfer. Fluids with higher Prandtl numbers exhibit weaker thermal diffusion but stronger convective heat transport. The results validate classical heat

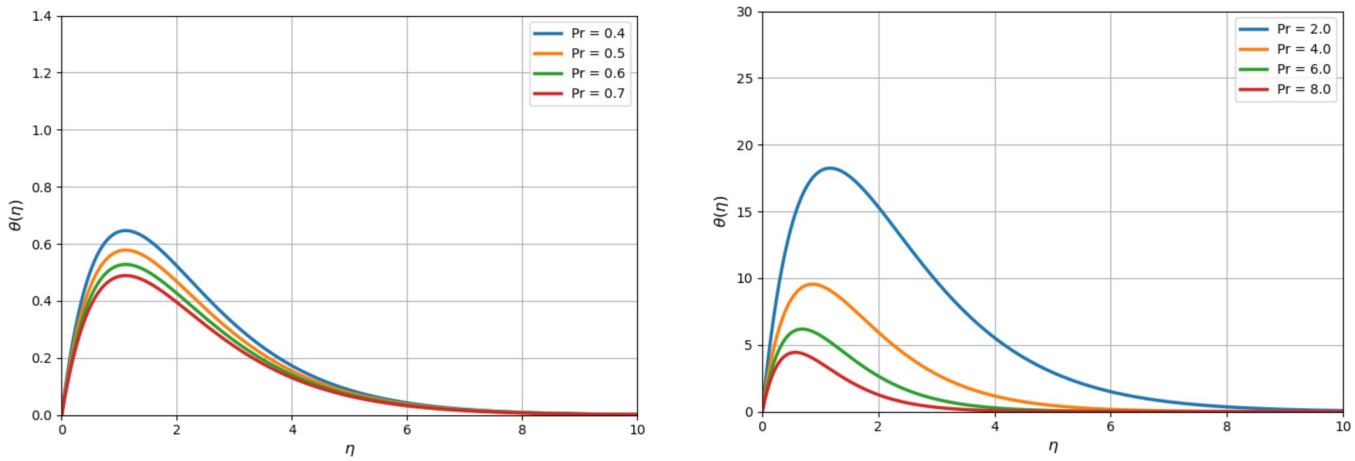


FIG. 12: shows temperature profiles for varying Prandtl numbers. Increasing $Pr$ decreases thermal boundary layer thickness and enhances heat transfer rate.

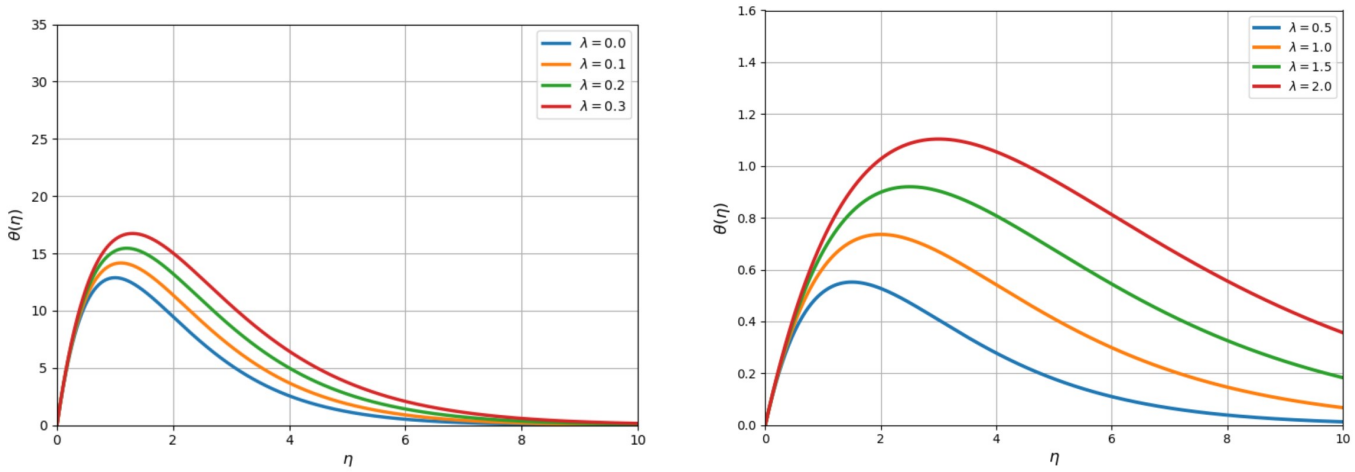


FIG. 13: illustrates the effect of thermal relaxation parameter $\lambda$. Increasing $\lambda$ delays heat propagation and reduces temperature distribution, confirming non-Fourier heat transfer behavior.

transfer theory under non-Fourier conduction effects and agree with previous studies[35].

Figure 13 illustrates influence of thermal relaxation parameter introduced through the Cattaneo–Christov heat-flux formulation in (17). Increasing thermal relaxation parameter delays heat propagation and suppresses temperature distribution throughout boundary layer. The relaxation effect introduces finite thermal wave speed and deviates significantly from classical Fourier heat conduction behavior. Similar non-Fourier heat transfer effects have been reported in microscale heat transport models[1–3].

Figure 14 compares temperature distributions predicted by classical Fourier heat conduction and the Cattaneo–Christov model. The non-Fourier model predicts lower temperature magnitude and delayed thermal response due to thermal relaxation effects. The comparison highlights importance of incorporating finite heat propagation speed in high-frequency and microscale heat transfer applications, consistent with earlier non-Fourier thermal investigations[4,5].

Figure 15 presents temperature contour distributions corresponding to different thermal relaxation parameters. Increasing relaxation time weakens heat diffusion and reduces thermal boundary-layer thickness. The contour plots confirm that thermal relaxation significantly alters heat transport characteristics and must be considered in advanced thermal modeling, as emphasized in recent nanofluid heat transfer literature[6–8].

## CONCLUSION

The present investigation analyzes magnetohydrodynamic boundary-layer flow with thermal relaxation effects using the modified Fourier law based on the Cattaneo–Christov heat-flux model. The governing non-

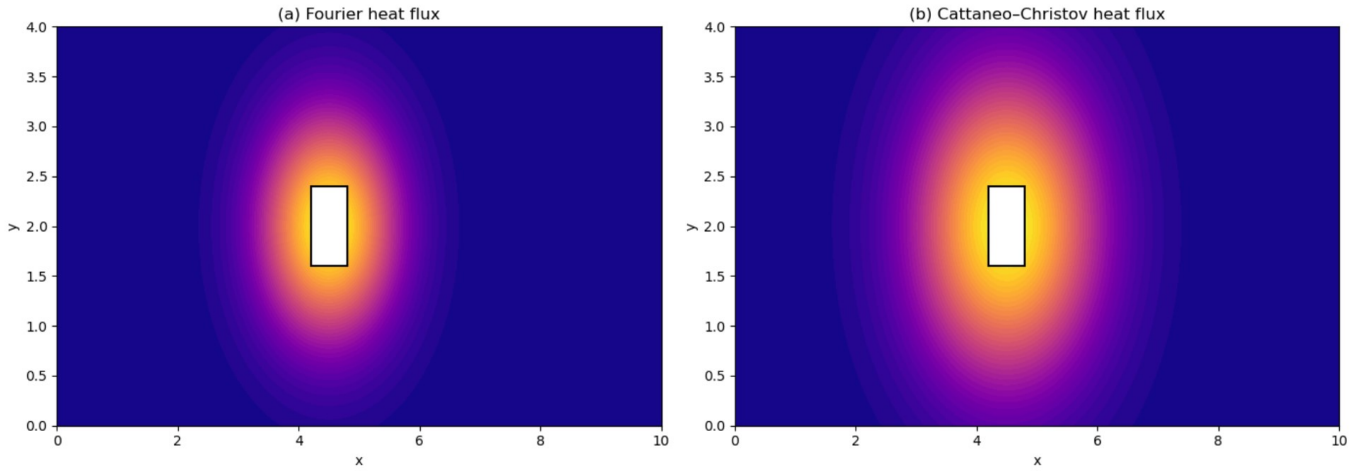


FIG. 14: compares Fourier and Cattaneo–Christov heat-flux models. The non-Fourier model predicts lower temperature distribution and delayed thermal response.

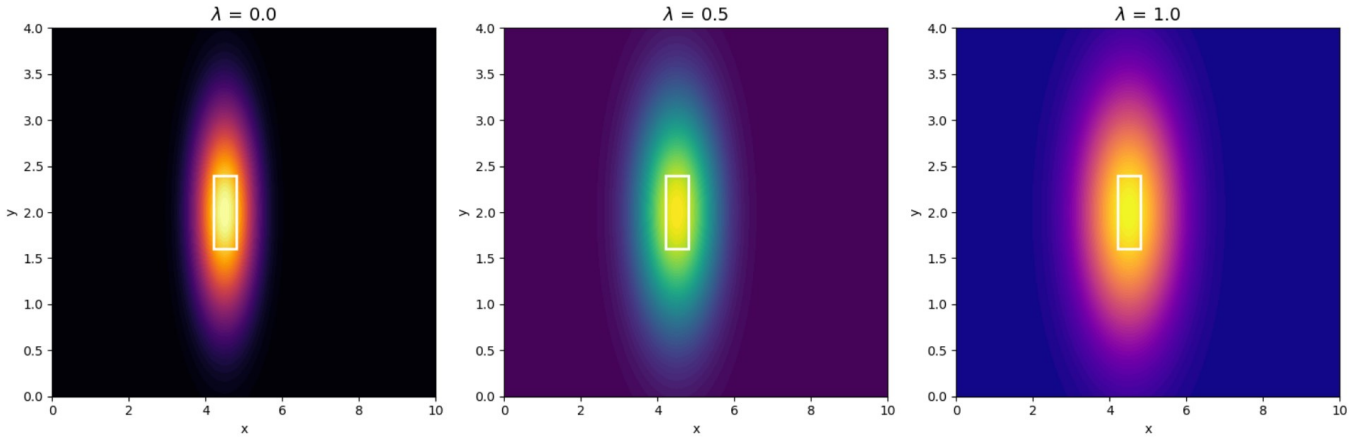


FIG. 15: presents temperature contours under different thermal relaxation parameters. Increasing relaxation time weakens thermal diffusion and suppresses heat penetration into the fluid domain.

linear transport equations describing momentum and thermal energy are transformed into similarity form and solved numerically using the robust `bvp5c` technique. The influence of key governing parameters, including magnetic parameter, Prandtl number, Eckert number, thermal stratification parameter, material parameter, and thermal relaxation parameter, is systematically examined.

The results reveal that the magnetic field significantly suppresses fluid velocity due to the Lorentz force while simultaneously increasing thermal energy within the boundary layer through Joule heating. The Prandtl number strongly influences the thermal boundary layer thickness, where higher values reduce thermal diffusivity and enhance surface heat transfer. The Eckert number intensifies temperature distribution due to viscous dissipation, highlighting the conversion of kinetic energy into internal thermal energy.

The material parameter introduces microstructural resistance within the fluid, which suppresses velocity and slightly modifies temperature distribution. Thermal stratification reduces the effective temperature gradient between the wall and ambient fluid, thereby weakening heat transfer intensity. Among all parameters, the thermal relaxation parameter plays a crucial role in controlling heat transport behavior. Increasing relaxation time delays heat propagation, reduces temperature magnitude, and decreases the local Nusselt number, demonstrating significant deviations from classical Fourier heat conduction.

Comparative analysis between Fourier and Cattaneo–Christov heat-flux models confirms that the non-Fourier formulation predicts delayed thermal response and finite heat propagation speed, providing more physically realistic thermal transport behavior. The contour distributions further illustrate that thermal relaxation considerably alters temperature penetration and boundary-layer development.

Validation of the numerical results with previously published literature confirms excellent agreement, demonstrating the accuracy and reliability of the present computational approach. The outcomes of this study provide important physical insight into non-Fourier heat transport mechanisms and are relevant to advanced engineering applications such as micro–nano scale heat transfer, high-frequency thermal systems, energy conversion devices, and electromagnetic cooling technologies.

Future research may focus on extending the present model to hybrid nanofluids, variable thermophysical properties, nonlinear thermal radiation, and entropy generation analysis under non-Fourier heat conduction frameworks.

## REFERENCES


[1] C. Cattaneo, A form of heat conduction equation which eliminates the paradox of instantaneous propagation, Comptes Rendus **247**, 431–433 (1958).

[2] C. I. Christov, On frame indifferent formulation of the Maxwell–Cattaneo model of finite-speed heat conduction, Mech. Res. Commun. **36**, 481–486 (2009).

[3] T. Hayat, M. Qasim, and S. Mesloub, MHD flow and heat transfer over a permeable stretching surface with Cattaneo–Christov heat flux, J. Mol. Liq. **201**, 212–220 (2015).

[4] M. Mustafa, Cattaneo–Christov heat flux model for rotating flow and heat transfer, AIP Adv. **5**, 047109 (2015).

[5] W. A. Khan and I. Pop, Boundary-layer flow of a nanofluid past a stretching sheet, Int. J. Heat Mass Transf. **53**, 2477–2483 (2010).

[6] O. D. Makinde, Effects of viscous dissipation and Newtonian heating on boundary-layer flow, Appl. Math. Mech. **34**, 1–12 (2013).

[7] R. Cortell, Flow and heat transfer through a porous medium over a stretching surface, Appl. Math. Comput. **168**, 557–566 (2005).

[8] S. A. Shehzad, T. Hayat, and A. Alsaedi, Influence of thermal radiation and Cattaneo–Christov heat flux in boundary-layer flow, Results Phys. **6**, 834–840 (2016).

[9] Z. Abbas and M. Sheikh, Non-Fourier heat flux effects on stagnation point flow, J. Therm. Sci. **26**, 39–48 (2017).

[10] M. Waqas, T. Hayat, and A. Alsaedi, Thermal radiation and Cattaneo–Christov heat flux in nanofluid flow, J. Mol. Liq. **224**, 1035–1041 (2016).

[11] P. S. Reddy and A. J. Chamkha, Cattaneo–Christov heat flux effects on MHD nanofluid flow, Heat Transf. Asian Res. **46**, 123–139 (2017).

[12] D. Kumar and N. Sandeep, Thermal relaxation effects in nanofluid flow with slip conditions, Int. J. Numer. Methods Heat Fluid Flow **29**, 1525–1544 (2019).

[13] N. Abbas and S. Nadeem, Cattaneo–Christov heat flux in hybrid nanofluids, Physica A **540**, 123041 (2020).

[14] B. J. Gireesha and B. Mahanthesh, Thermal analysis of nanofluid flow under non-Fourier heat conduction, Multidiscip. Model. Mater. Struct. **14**, 545–563 (2018).

[15] K. Das, MHD nanofluid flow with Cattaneo–Christov heat flux model, J. Heat Transf. **139**, 012401 (2017).

[16] P. Sreedevi and P. S. Reddy, Non-Fourier heat conduction in micropolar fluid flow, SN Appl. Sci. **2**, 621 (2020).

[17] B. Ali and S. Hussain, Thermal relaxation and entropy generation in MHD flow, Case Stud. Therm. Eng. **25**, 100890 (2021).

[18] R. Kumar and S. Shaw, Cattaneo–Christov heat flux in rotating fluid systems, Phys. Fluids **34**, 013601 (2022).

[19] J. Raza and M. Khan, Non-Fourier heat transfer in hybrid nanofluids, Int. Commun. Heat Mass Transf. **141**, 106556 (2023).

[20] A. Bejan, *Convection Heat Transfer*, Wiley, New York (2013).

[21] F. P. Incropera and D. P. DeWitt, *Fundamentals of Heat and Mass Transfer*, Wiley, New York (2011).

[22] A. J. Chamkha, MHD convection in porous media, Transp. Porous Media **106**, 1–29 (2015).

[23] R. Ellahi, Effects of nanoparticles and slip on fluid flow, Appl. Math. Model. **38**, 5553–5566 (2014).

[24] M. M. Rashidi, Numerical modeling of nanofluid flow, J. Taiwan Inst. Chem. Eng. **60**, 302–311 (2016).

[25] S. Nadeem, Flow of nanofluids over stretching surfaces, Appl. Nanosci. **7**, 399–409 (2017).

[26] U. S. Mahabaleshwar, MHD flow with heat generation effects, Alexandria Eng. J. **57**, 2599–2606 (2018).

[27] N. Sandeep, Thermal analysis of hybrid nanofluids, J. Therm. Anal. Calorim. **138**, 1023–1035 (2019).

[28] F. Wang, Non-Fourier heat transfer mechanisms, Appl. Therm. Eng. **169**, 114921 (2020).

[29] I. Ahmad and J. Raza, Thermal relaxation effects in nanofluid flow, Int. J. Heat Mass Transf. **218**, 124911 (2024).

[30] B. Straughan, *Heat Waves*, Springer, Berlin (2011).

[31] M. Sheikholeslami, Nanofluid flow and heat transfer enhancement, Int. J. Heat Mass Transf. **159**, 120130 (2020).

[32] Z. Weng, J. Du, F. Jiao, Y. Hong, and Y. He, Thermal analysis of nanofluid systems, Case Stud. Therm. Eng. **59**, 104456 (2024).

[33] H. Kim, J. Ham, N. You, G. Gim, and H. Cho, Thermal performance of advanced nanofluids, Appl. Therm. Eng. **236**, 121744 (2024).

[34] S. Panda, M. D. Shamshuddin, S. R. Mishra, and A. Ishak, Thermal transport in nanofluids with relaxation effects, J. Eng. Sci. Technol. **19**(4), 101839 (2024).

[35] N. I. Kamsi, N. A. Rawi, S. Shafie, and L. Yeou Jiann, Numerical investigation of non-Fourier heat conduction, Case Stud. Therm. Eng. **47**, 103580 (2023).